1st International Conference on Sensing Technology
November 21-23, 2005 Palmerston North, New Zealand

A Comparison of Pull-in Voltage Calculation Methods for MEMS-Based Electrostatic Actuator Design

Sazzadur Chowdhury, M. Ahmadi, W. C. Miller
Department of Electrical and Computer Engineering
University of Windsor
Windsor, Ontario, N9B 3P4
Canada

Abstract

A comparative study of closed-form methods for calculating the pull-in voltage of electrostatically actuated fixed-fixed beam actuators has been presented. Five different pull-in voltage calculation methods have been considered in the analysis. For wide beams in the small deflection regime where the fringing field effects and stress induced nonlinear stretching can be neglected, the performance of all the five methods are reasonably satisfactory with a maximum deviation of 2.6% from the CoSolve FEA results. For narrow beams in the small deflection regime, maximum deviation from Architect™ parametric analysis results is about 20%. For wide beams in the large deflection regime, four out of the five models evaluated pull-in voltages are about one-fourth the values when compared with CoventorWare™ and Architect™ results. It has been observed that proper modeling of the fringing field capacitances and the stress induced nonlinear spring hardening effects are the key factors to improve the accuracy of a closed-form method.

Keywords: MEMS, Electrostatic, Sensor, Actuator, Fixed-Fixed Beam, Pull-in Voltage.

1 Introduction

MEMS-fabricated fixed-fixed beam geometry electrostatic actuators are widely used to realize high performance microresonators, microfabricated RF switches, grating light valves for optical switching and projection displays, and measurement of material properties of microfabricated thin films, etc. [1-4]. The drive mechanism of these devices includes a constant voltage source (voltage drive) or constant current source (current drive) to enable electrostatic actuation or capacitive sensing [5]. Most electrostatic MEMS devices are of constant voltage drive type due to this mode's relative ease of implementation [6]. The electrostatic force associated with the constant voltage drive mode is nonlinear and gives rise to the well-known phenomenon of 'pull-in'. The pull-in phenomenon causes an electrostatically actuated beam or diaphragm to collapse on the ground plane if the drive voltage exceeds certain limit depending on the device geometry. Accurate determination of the pull-in voltage is critical in the design process to determine the sensitivity, frequency response, instability, distortion, and the dynamic range of the device [5].

3-D electromechanical finite element analysis (FEA) can predict the pull-in voltage with a very high degree of accuracy; however, the method is computationally intensive and even the finite difference methods can be less efficient if the structure is complex. The results from Architect™—a parametric behavioral model recently developed by the Coventor, Inc., are within 5% agreement with the FEA results [7]. To expedite the design process, fast analytical and empirical closed-form solutions have been developed by many authors. Unfortunately, the accuracy of the different methods varies widely depending on the device specifications and modeling parameters, such as the fringing field considerations, presence of residual stress, small deflection, or large deflection, etc. In this paper a comparative study has been carried out to determine the accuracy level of five pull-in voltage calculation methods. The results from these methods have been compared with definitive Finite element analysis results and percent variations have been determined. Analysis shows that, the methods that account for affects of the fringing field capacitances and the stress induced nonlinear spring hardening effects in an appropriate manner can predict the pull-in voltage with a higher degree of accuracy compared to the others.

2 Fixed-Fixed Beam Geometry Electrostatic Actuator

A conceptual diagram of a fixed-fixed beam geometry electrostatic actuator is shown in figure 1a. The beam is of length l, width w, area $A = wl$, thickness h, and is separated from a fixed ground plane by an initial airgap thickness d_0. Following assumptions are made to characterize the beam:

1. The beam is of uniform rectangular cross-section and is fabricated with a perfectly conducting homogeneous material.
2. The beam is initially planar and parallel to the fixed ground plane and has exact fixed boundary

conditions (all six degrees of freedom at each boundary are clamped).

3. The beam dimensions are within the Bernoulli-Euler limit ($l >> w$ and $l >> h$). This assumption allows neglecting the shear stresses near the fixed supports and approximating the stress in the beam as purely uniaxial along the beam length [4].
4. The beam has negligible stress gradient along its length.
5. The structure operates in vacuum—which is equivalent to negligible atmospheric loading [8].
6. The width of the supporting dielectric spacers is large enough so that any fringing fields originating at the ends of the support structures do not influence the deflection of the suspended length l of the beam. Thus, the total capacitance between the beam and the fixed ground plane consists of three components: the parallel plate capacitance, the fringing field capacitance due to the beam width, and the fringing field capacitance due to the thickness of the beam.

When actuated by a constant drive voltage V, the developed electrostatic force attracts the beam toward the fixed ground plane. As both ends of the beam are fixed, unlike the parallel plate actuator, a higher charge concentration occurs in the middle region of the beam compared to the regions near to the fixed ends. Consequently, the beam experiences a higher force in the middle region compared to the fixed ends.

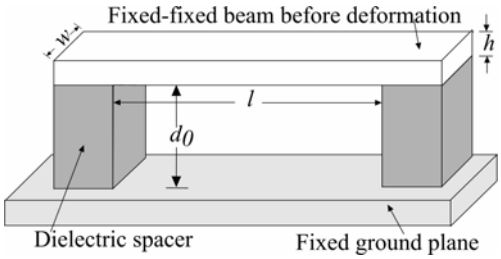

(a)

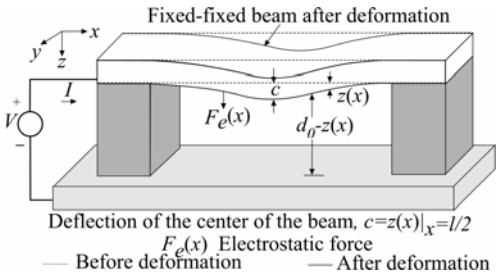

(b)

Figure 1: (a) Conceptual diagram of a fixed-fixed beam separated from a fixed ground plane by dielectric spacers. (b) A conceptual diagram showing the deformation profile of the beam due to an electrostatic force when biased oppositely by a constant drive voltage.

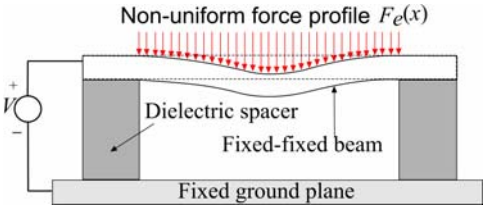

Figure 2: Non-uniform force profile of an electrostatically actuated fixed-fixed beam

This non-uniform force, as shown conceptually in figure 2, causes a position dependent deflection $z(x)$ along the beam axis. The non-uniformity of the electrostatic force increases as the beam deforms further toward the fixed ground plane. For any given electrostatic force, the maximum deflection c of the beam occurs at the center ($c = z(x)\big|_{x=l/2}$) of the beam (figure 1b). At static equilibrium, the electrostatic attraction force is counterbalanced by the elastic restoring force. During operation, if the electrostatic force due to an increased drive voltage overcomes the elastic restoring force, the equilibrium is lost and the beam collapses on the fixed ground plane due to the 'pull-in' phenomenon.

3 Pull-in Voltage Models

Different approaches have been made to develop closed form models to determine the pull-in voltages of electrostatically actuated fixed-fixed beam geometry actuator. Five (5) most significant ones in terms of accuracy are listed below:

3.1 Parallel Plate Approximation

The simple parallel-plate approximation method assumes that the beam has a linear spring constant, considers a piston like motion, and predicts that the pull-in occurs when the highest deformation exceeds one-third of the airgap. This analysis neglects the affects of the fringing field capacitances and excludes the nature of the fixed boundary conditions, non-uniformity of the electrostatic pressure due to charge redistribution, affects of the residual stress, and the developed nonlinear stress distribution due to the stretching of the beam. For wide beams with small airgaps, errors up to 20% have been reported in literature due to such approximations [4]. For large deflections or extreme fringing field cases, the errors are much higher. The pull-in voltage for this ideal structure is expressed as [3]:

$$V_{PI} = \sqrt{\frac{8Kd_0^3}{27\varepsilon_0 A}} \qquad (1)$$

where K is the linear spring constant, ε_0 is the permittivity of free space, d_0 is the initial airgap, and A is the area of the exposed faces of the parallel plates.

3.2 Natural Frequency Approach

In [9] a lumped element spring-mass system has been used to derive an analog equivalent electrical one-port network of a fixed-fixed beam microresonator. The fundamental frequency of the system has been determined as a function of the voltage and the pull-in voltage has been determined from the fact that at pull-in, the fundamental frequency drops to zero. Following this approach, the pull-in voltage can be expressed as:

$$V_{PI} = 10.7\left\{\frac{\hat{E}Id_0^3}{\varepsilon_0 Al^3}\left[1+0.295\varepsilon(1-\nu^2)\left(\frac{l}{h}\right)^2\right]\right\}^{1/2} \quad (2)$$

where $\hat{E}$ is the effective Young's modulus, I is the moment of inertia, ε is the strain, and ν represents the Poisson ratio.

3.3 Energy method

The method proposed in [10] uses the energy stored in a capacitor formed by a fixed-fixed beam and a fixed ground plane to determine the pull-in voltage of the structure. In [10], the pull-in phenomenon has been defined as the condition when the second derivative of the total potential energy stored in the beam equals to zero. Following [10], the pull-in voltage can be expressed as:

$$V_{PI} = \frac{c_1\pi^2}{l^2}\left[\frac{\hat{E}Id_0^3}{w\varepsilon_0}\left(1+c_2\frac{Nl^2}{\hat{E}I}\right)\right]^{1/2} \quad (3)$$

where c_1 and c_2 are two constants. In [12], the values of c_1 and c_2 have been determined as $c_1 = 1.199$ and $c_2 = 0.0246$. In equation (3), N represents the tension axial force which is expressed as [3] $N = hw\hat{\sigma}_0$, where $\hat{\sigma}_0$ is the effective residual stress. The energy method does not account for the increase in the fringing field capacitances due to a decreasing beam width. In [10], the authors considered the large deflection behavior of the beam while determing the resonant frequency; however, the nonlinear stretching of the beam during large deflection was not included in the expression to calculate the pull-in voltage.

3.4 Two (2)-D Model

A simple and fast empirical solution to determine the pull-in voltage for cantilever beams, fixed-fixed beams and circular diaphragms with excellent accuracies is available in [4]. The closed-form solution, known as the 2-D model, can determine the pull-in voltages for structures subjected to small deflection within 1.5% of the FEA results in the small deflection regime. The 2-D model was derived first by determining three fitting parameters (γ_{1n}, γ_{2n}, and γ_{3n}) using a least-square data fitting technique to a large sample of experimentally measured pull-in voltages for structures with varying geometrical dimensions and material properties. These fitting parameters are then used in conjunction with the effective spring constants to derive the following general pull-in voltage expression for a fixed-fixed beam geometry actuator:

$$V_{PI} = \sqrt{\frac{\gamma_{1n}S}{\varepsilon_0 l^2 D_n(\gamma_{2n},k,l)}\left[1+\gamma_{3n}\frac{d_0}{w}\right]} \quad (4)$$

where

$$\left.\begin{aligned} &D_n = 1+\frac{2\{1-cosh(\gamma_{2n}kl/2)\}}{(\gamma_{2n}kl/2)\,sinh(\gamma_{2n}kl/2)} \\ &k = \sqrt{12S/B}\;;\; S = \hat{\sigma}_0 h d_0^3;\; B = \hat{E}h^3 d_0^3 \\ &\text{and}\;\; \gamma_{1n} = 2.79\,,\; \gamma_{2n} = 0.97 \;\text{and}\; \gamma_{3n} = 0.42 \end{aligned}\right\} \quad (5)$$

3.5 IMEC Model

The model presented in [11] is known as the IMEC model and includes the effects of partial electrode configuration, axial stress, non-linear stiffening, charge redistribution, and the fringing field effects to determine the pull-in voltage for fixed-fixed beams. Following [11], the pull-in voltage for a fixed-fixed beam subjected to a uniformly distributed transverse load along the entire beam length can be expressed as:

$$V_{PI} = \left[\frac{8K_{eff}d_0^3}{20.9\varepsilon_0 l w_{eff}}\right]^{1/2} \quad (6)$$

where

$$\left.\begin{aligned} &K_{eff} = \frac{32\hat{E}wh^3}{l^3}+\frac{\xi N}{l};\; 8\le\xi\le 9.6 \\ &k_0 = \left[\frac{12N}{\hat{E}wh^3}\right]^{1/2} \\ &N = hw(\hat{\sigma}_0+\pi^2 E(\beta d_0)^2/4l^2 \\ &w_{eff} = w[1+0.65(1-\beta)d_0/w]\,,\;\text{and}\;\beta = 0.4\,. \end{aligned}\right\} \quad (7)$$

In [11], it has been suggested to use $\xi = 8.32$ in (7) for MEMS devices that satisfies the condition $0.2 < k_0 l/4 < 40$.

3.6 Potential Energy Method

In [12], the total potential energy content of a fixed-fixed beam subjected to electrostatic force is used to determine the pull-in voltage without the fringing field effects and then a correction factor is applied to account for the fringing field effects. The first-order fringing field effects have been approximately compensated by an effective beam width. Following [12], the pull-in voltage can be calculated from:

$$V_{PI} = \sqrt{\frac{1}{1+0.65d_0/w}} \times \sqrt{c_1 \frac{\hat{E}h^3 {d_0}^3}{\varepsilon_0 l^4} + c_2(1-v)\frac{{d_0}^3 h\hat{\sigma}_0}{\varepsilon_0 l^2}} \quad (8)$$

where the constants $c_1 = 11.7$ and $c_2 = 3.6$.

4 Comparison of Different Pull-in Voltage Calculation Methods

In this section, all the five closed-form methods described in the previous section have been compared for a wide range of device dimensions and deflection characteristics. For each category, results from published definitive FEA results have been used as the reference value and percent deviations from the FEA results were determined.

4.1 Wide Beams in Small Deflection

A beam is considered wide when $w \geq 5h$ [4]. Wide beams exhibit plane-strain conditions and the effective Young's modulus $\hat{E}$ for a wide beam becomes the plate modulus which is expressed as $\hat{E} = E/(1-v^2)$ where E is the Young's modulus. The effective residual stress for a fixed-fixed beam in the Bernoulli–Euler limit is expressed as $\hat{\sigma} = \sigma_0(1-v)$ [4]. For a high value of w/d_0 (wide beams with small airgaps), the fringing fields can be neglected and the total capacitance approaches to that of a parallel plate model. Seven test cases as listed in Table 1 have been used to calculate the pull-in voltages using the different methods. It is to be noted here that in [13], these seven test cases have been compared with CoSolve (CS) FEA results and were verified to be in good agreement with experimentally measured values. It is also to be noted that [4] and [13] present the same model; however, [13] includes one more test case result. This makes this data set a reasonable basis of comparison. The comparison results are presented in Table 2 and the percent differences from the CS FEA results are listed in Table 3. Tables 2 and 3 show that for wide beams in the small deflection regime, where the fringing field effects are negligible, the results from the different closed-form methods used in the analysis are very much within the acceptable limits of a closed-from solution. From Table 3, [13] has the lowest deviation (1.5%) from the CS FEA results whereas [9] shows the highest deviation (13.17%) from the CS FEA results.

Table 1: Test case specifications for fixed-fixed beam pull-in analysis: E=169 GPa, w=50 μm, h=3 μm, d_0=1 μm. (length is in meters, residual stress is in MPa).

Device Parameters	Case 1	Case 2	Case 3	Case 4	Case 5	Case 6	Case 7
Beamlength l	250	250	250	250	350	350	350
Poisson ratio v	0.06	0.32	0.06	0.06	0.06	0.06	0.06
Residual stress σ_0	0	0	100	-25	0	100	-25

4.2 Narrow Beams in Small Deflection and Wide Beams in Large Deflection

A beam is considered narrow when $w < 5h$. In this case, the effective Young's modulus $\hat{E}$ is simply the Young's modulus E [4]. The fringing field increases with a decreasing w/d_0 and for extreme cases (very small w/d_0 as in the case of a narrow beam), the fringing field capacitances become the dominant one and can increase the overall capacitance by a factor of 3 [14]. To compare the closed-form methods for narrow beams in the small deflection regime and wide beams in the large deflection regime, two test cases having same device specifications as in [11] have been used and the results are compared with the published results from the Architect™ parametric analysis module [7] and CoventorWare™ (CW) FEA [11] results. The device specifications are listed in Table 4 and the percent difference from the Architect™ parametric analysis module [7] and CW FEA [11] results are summarized in Tables 5 and 6. It is observed that Table 6 is in sharp contrast with Table 3 with a wide variation of the percent differences. Since the energy method [10] doesn't include any parameter to account for the affects of the fringing fields, the model obviously fails to account for any variation in the electrostatic pressure originating from the fringing field

Table 2: Pull-in voltages from different closed-form methods and CS FEA for the 7 test cases listed in Table 1

Method	Pull-in Voltage V_{PI} (Volts)						
	Case 1	Case 2	Case 3	Case 4	Case 5	Case 6	Case 7
CoSolve FEA [13]	40.1	41.2	57.6	33.6	20.3	35.8	13.7
Ref. [9]	35.55	37.44	48.31	30.1	18.14	32.5	12.1
Ref. [10]	39.31	41.42	57.45	33.26	20.06	36.02	13.35
Ref. [11]	40.38	42.54	58.87	34.12	20.60	36.77	13.63
Ref. [12]	39.10	41.20	56.85	33.22	19.95	35.6	13.45
Ref. [13]	39.5	41.5	56.9	33.7	20.20	35.40	13.8

Table 3: Δ% between pull-in voltages calculated using five (5) different closed-form methods and the CS FEA Results [13] for the test cases listed in Table 1

Between	Δ%						
	Case 1	Case 2	Case 3	Case 4	Case 5	Case 6	Case 7
Ref. [9]-CoSolve	12.82	10.02	11.00	11.62	11.94	10.06	13.17
Ref. [10]-CoSolve	2.0	0.52	0.26	1.02	1.22	0.62	2.60
Ref. [11]-CoSolve	0.69	3.16	2.15	1.54	1.46	2.63	0.50
Ref. [12]-CoSolve	2.54	0.01	1.32	1.14	1.74	0.59	1.84
Ref. [13]-CoSolve	1.5	0.70	1.20	0.30	0.50	1.1	0.70

Table 4: Pull-in voltage comparison for a narrow beam in the small deflection regime and a wide beam in the large deflection regime. Common parameters: E=77 GPa, v=0.33, σ_0 =0, l =300 μm.

Specifications	Case	
	8	9
Width, w (μm)	0.5	50.0
Beam thickness, h (μm)	1.0	0.5
Airgap thickness, d_0 (μm)	1.0	6.0
w/d_0	0.5	8.33
h/d_0	1.0	0.0833

Table 5: Pull-in voltage from different closed-form models, CW FEA, and Architect™ for the test cases listed in Table 4.

Method	Pull-in Voltage V_{PI} (Volts)	
	Case 8	Case 9
CW FEA [11]	2.50	89.60
Architect™ [7]	2.81	90.00
Ref. [9]	3.2	17.61
Ref. [4]	2.63	19.17
Ref. [10]	3.54	19.48
Ref. [11]	2.87	79.93
Ref. [12]	2.33	18.79

Table 6: Δ% of the closed-form model pull-in voltages from CW FEA and Architect™ results for test cases listed in Table 4.

Between	Δ%	
	Case 8	Case 9
CW FEA [11] and Architect™ [7]	12.4	0.44
Ref. [4] and CW FEA [11]	4.94	367.50
Ref. [4] and Architect™ [7]	6.84	369.58
Ref. [9] and CW FEA [11]	21.88	408.58
Ref. [9] and Architect™ [7]	12.2	410.02
Ref. [10] and CW FEA [11]	29.37	359.86
Ref. [10] and Architect™ [7]	20.61	361.33
Ref. [11] and CW FEA [11]	13.02	12.10
Ref. [11] and Architect™ [7]	2.24	12.60
Ref. [12] and CW FEA [11]	6.97	376.84
Ref. [12] and Architect™ [7]	20.24	378.96

capacitances that increases with a decreasing w/d_0; however, for a very small h/d_0 (Table 4, case 9, $h/d_0 = 0.083$), the difference from the CW FEA result is very high (~360%). In [10], it was mentioned that the model is valid only for the small deflection regime. Thus, case 9 is beyond the claimed region of validity of that model. Apparently, the method doesn't account for the affects of the nonlinear stretching of the beam during large deflection and that may be the reason for a large difference.

For the extreme fringing field case in the small deflection regime (Table 4, case 8), the model in [11] has a difference of 13% with the CW FEA. Some additional analysis by Coventor shows that the pull-in voltage should be closer to 2.9 V rather than 2.5 V for this case [7]. Coventor explains that this anomaly in FEA is partly due to the shape of the cross section which has violated the plate assumption used for the Young's modulus and needs correction whereas Architect™ and the model in [11] handle this well [7]. In [11] it was recognized that the under-estimation of the nonlinear stiffening causes errors, but also the over-estimation when partial electrodes are used. The use of the Beta correction coefficient in [11] is the cause for some concern with some of the simulations. The performance of the potential energy method [12] is the poorest for both the extreme fringing field and the large deflection cases.

Above analysis of the different closed-form methods reveals that proper modeling of the electrostatic force due to the fringing field capacitances and the nonlinear characteristics of the beam stiffness are the key factors contributing to the accuracy of the closed-form models to determine the pull-in voltage of electrostatically actuated fixed-fixed beams. The IMEC model (11) performs best in both small and large deflection regimes for both wide and narrow beams since the model accounts for the fringing field capacitances and also the nonlinear stretching when the beam undergoes large deflection. The only weakness of this model is the confusion with the Beta correction factor than Coventor discussed in detail [7]. This Beta correction factor may also be reason of a little higher deviation in the small deflection for wide beams. Without the fringing field correction, for case (8), the IMEC model determined pull-in voltage is about 26% in error with the Architect result and without the stretching term the deviation from Architect result is about 351% similar to that from [4], [10] and [12]. Additionally, if the nonlinear stretching term [11] is included in the axial tension expression, the authors found that the accuracy of the

model presented in [10] improves significantly (within 9.6% from the CW FEA result for case 9 in contrast to a value which is nearly one-fourth of the CW FEA value when the stretching term is neglected). The first-order fringing field correction that has been used in some models; improves the accuracy; however, analysis shows that this approximation is inadequate when the fringing field is extreme. Apparently, omission of the beam thickness in the expression to evaluate the effective beam width, as done in the first-order fringing field correction, is the cause of this inaccuracy.

5 Conclusions

A comparative study has been carried out to determine the relative accuracy of five closed-form models used to determine the pull-in voltage of a fixed-fixed beam electrostatic actuator. Nine test cases have been considered and in each case published definitive FEA result or experimentally verified data have been used as the reference. For each case percent variation from the reference FEA result has been determined. From the analysis it is evident that in the small deflection regime, the 2-D model [4] has the highest accuracy with a maximum deviation of only 1.5 % from the experimentally verified CoSolve FEA results. For narrow beams (extreme fringing field case) in the small deflection regime the IMEC model [11] performs much better compared to the other models. For wide beams in the large deflection regime, the IMEC model is much superior compared to all other models with a deviation from FEA results of about 12 percent. It has been determined that appropriate modeling of the fringing fields and nonlinear stretching are the key factors to improve a model's accuracy.

6 Acknowledgements

This research has been supported by the Natural Sciences and Engineering Research Council of Canada (NSERC), CMC Microsystems, MICRONET Canada, and the Gennum Corporation of Burlington, Ontario.

7 References

[1] S. Pourkamali, A. Hashimura, R. Abdolvand, G. K. Ho, A. Erbil, and F. Ayazi, "High-Q Single Crystal Silicon HARPSS Capacitive Beam Resonators with Self-Aligned Sub-100-nm Transduction Gaps", *Journal of Microelectromechanical Systems*, Vol. 12, No. 4, pp. 487-496, Aug. 2003.

[2] M. Hill, C. O'Mahony, R. Duane, and A. Mathewson, "Performance and reliability of post-CMOS metal/oxide MEMS for RF application", *Journal of Micromech. and Microengr.*, Vol. 13, No. 4, pp. 131-138, Jul. 2003.

[3] S. D. Senturia, "Microsystems Design", Kluwer Academic Publishers, Boston, 2000, pp. 249-259.

[4] P. M. Osterberg and S. D. Senturia, "M-TEST: A Test Chip for MEMS Material Property Measurement Using Electrostatically Actuated Test Structures", *Journal of Microelectromechanical Systems*, Vol. 6, No. 2, pp. 107-118, Jun. 1997.

[5] R. Puers and D. Lapadatu, "Electrostatic Forces and their Effects on Capacitive Mechanical Sensors", Sensors and Actuators A, Vol. 56, No. 3, pp. 203–210, Sept. 1996.

[6] Pons-Nin, A. Rodriguez, and L. M. Castaner, "Voltage and Pull-in in Current Drive of Electrostatic Actuators", *Journal of Microelectromechanical Systems*, Vol. 11, No. 3, pp. 196-205, Jun. 2002.

[7] Coventor, Inc., "Pull-in Voltage Analysis of Electrostatically-Actuated Beams Verifying Accuracy of Coventor Behavioral Models", Available. [Online]. http://www.coventor.com/ media/ fem_comparisons/ pullin_voltage.pdf .

[8] Ladabaum, X. Jin, H. T. Soh, A. Atalar and B. T. Khuri-Yakub, "Surface Micromachined Capacitive Ultrasonic Transducers", Transactions on Ultrasonics, Ferroelectrics, and Frequency Control, Vol. 45, No. 3, May 1999, pp. 679-690.

[9] D. J. Ijntema and H. A. C. Tilmans, "Static and Dynamic Aspects of an Air-gap Capacitor", *Sensors Actuators* A, Vol. 35, No. 2, pp. 121–128, Dec. 1992.

[10] H. A. C. Tilmans and R. Legtenberg, "Electrostatically driven vacuum-encapsulated polysilicon resonators: Part II. Theory and Performance", *Sensors Actuators A*, Vol. 45, No. 1, pp. 67–84, Oct. 1994.

[11] S. Pamidighantam, R. Puers, K. Baert and H. A. C. Tilmans, "Pull-in voltage analysis of electrostatically actuated beam structures with fixed–fixed and fixed–free end conditions", *Journal of Micromech. and Microengr*, Vol. 12, No. 4, pp. 458–464, Jul. 2002.

[12] C. O'Mahony, M. Hill, R. Duane, and A. Mathewson, "Analysis of Electromechanical Boundary Effects on the Pull-in of Micromachined Fixed–Fixed Beams", *Journal of Micromech. and Microengr*, Vol. 13, No. 4, pp. 75–80, Jul. 2003.

[13] P. M. Osterberg, "Electrostatically Actuated Microelectromechanical Test Structures for Material Property Measurements", *Ph.D. Dissertation*, MIT, Cambridge, MA, 1995, pp. 52-87.

[14] J. M. Rabaey, *Digital Integrated Circuits*, Prentice-Hall Inc., New Jersey, 1996, pp. 438-445.